Hindawi
Advances in Polymer Technology
Volume 2022, Article ID 5602902, 15 pages
https://doi.org/10.1155/2022/5602902

Research Article

Influence of Carbon Dioxide on the Glass Transition of Styrenic and Vinyl Pyridine Polymers: Comparison of Calorimetric, Creep, and Rheological Experiments

Felix Harden, Mahboubeh Kargar, and Ulrich A. Handge

Helmholtz-Zentrum Hereon, Institute of Membrane Research, Max-Planck-Strasse 1, 21502 Geesthacht, Germany

Correspondence should be addressed to Ulrich A. Handge; ulrich.handge@tu-dortmund.de

Received 17 May 2022; Accepted 31 August 2022; Published 3 October 2022

Academic Editor: Milan Mari

The glass transition of amorphous polymers determines the mobility of polymer chains and the time scale of relaxation processes. The glass transition temperature is reduced by the presence of low molecular weight molecules, e.g., dissolved gases or organic solvents. The quantitative knowledge of reduction of the glass transition temperature caused by the addition of carbon dioxide in a polymer melt is highly relevant for foam extrusion. However, measurement of the reduction of glass transition temperature caused by gas loading has to be performed under elevated pressure which implies high experimental efforts. In this work, we discuss and compare three methods for determination of the influence of carbon dioxide on thermal properties of amorphous polymers, i.e., calorimetric measurements, creep tests, and rheological experiments. The advantages and disadvantages of these methods are elucidated. Furthermore, the influence of molecular structure of the styrenic and vinylpyridine polymers on the glass transition temperature is discussed. Polystyrene generally shows the highest reduction of glass transition temperature. Poly(2-vinylpyridine) and poly(4-vinylpyridine) show a slightly less pronounced behaviour in comparison to polystyrene because of the lower polarity of polystyrene. Poly(α-methyl styrene) is associated with a different dependence of glass transition temperature on gas loading in calorimetric and rheological experiments.

1. Introduction

The glass transition temperature of an amorphous polymer is a material-specific value which is closely associated with the free volume and determines chain mobility and relaxation times [1]. Solution of low molecular weight molecules, e.g., an inert gas such as carbon dioxide (CO_2), in an amorphous polymer generally leads to a decrease of the glass transition temperature [2, 3]. Besides fundamental interest, this phenomenon is of high relevance in a number of polymer applications. The viscosity reduction in foam extrusion using physical blowing agents is a prominent example [4, 5]. In addition, the crystallization temperature of semicrystalline polymers is affected by gas loading [4]. Furthermore, polymer gas separation membranes may be influenced by the plasticization effect caused by gas solubility [6].

Depending on the applied temperature and pressure, low molecular weight molecules are dissolved in the polymer up to a maximum value which is termed solubility. Generally, the solubility increases with applied pressure. Before complete saturation at a specific applied pressure is achieved, diffusion describes the transport of the low molecular weight species in the polymer [7]. The solubility and diffusion coefficient of different gases in various polymers have been studied by several researchers [8, 9]. For example, the experimental determination of solubility and the diffusion coefficient of carbon dioxide in polymers is the subject of various works [10, 11]. Furthermore, numerical studies on Fickian and non-Fickian diffusion have been also performed [12].

In principal, one would need to separate the effects of hydrostatic pressure and gas loading on the thermal, mechanical, and rheological properties of polymers. Generally, the effect of pressure alone mainly becomes relevant at pressures much larger than 100 bar. Several techniques for rheological experiments at a high pressure have been developed [13]. The pressure coefficient for a variety of polymers

has been determined by several authors using different type of rheometers [14–16]. Different approaches in order to fit the experimental data were chosen [17]. A multipass rheometer has been also used for such experiments [18]. A recent review on this topic is given by Münstedt [19]. Generally, the pressure coefficient of amorphous polymers decreases with increasing temperature, whereas this trend has been shown to be less pronounced for a specific polyolefin which belongs to the class of semicrystalline polymers [19].

The zero shear rate viscosity of melts of amorphous polymers depends on temperature, applied pressure, and gas loading. The value of viscosity strongly increases in the vicinity of the glass transition temperature. A number of publications are devoted to rheological experiments of gas-loaded polymer melts under high pressure and quantified the viscosity reduction caused by gas loading [13, 20, 21]. Various works discussed the change of relaxation times and the viscosity reduction with gas loading [20–22]. Using a hyperbolic die, the planar elongational viscosity of a gas-loaded polystyrene melt has been measured by Wang et al. [23] In their work, it was shown that in addition to the shear viscosity, the extensional viscosity of polystyrene is also reduced by addition of carbon dioxide. Since a uniform extensional flow for a gas-loaded polymer melt can only be achieved with high experimental efforts, an elaborated calculation technique for the experimental data was applied in their work.

Because of its fundamental and technological relevance, several techniques have been developed for measuring the glass transition temperature of polymers under elevated pressure and gas loading. Calorimetric measurements under high pressure have been established by several researchers [3, 24]. The measurements of Huang et al. in the pressure range of up to 300 bar reveal that the phase transition of carbon dioxide can be observed in differential scanning calorimetric experiments [25]. The combination of Calvet calorimetry and pressure drop method allows for the simultaneous measurement of solubility and diffusion coefficient [26].

A pioneering work has been performed by Wang et al. who carried out tensile creep tests under gas loading and elevated pressure [27]. In their experiments, the maximum test temperature was 45°C. The authors quantified the shift of the glass transition temperature of polystyrene caused by carbon dioxide and elucidated the experimental phenomenon. Further creep experiments have been carried out by Condo and Johnston [28]. Their data also reveal the increase of creep compliance for poly(methyl methacrylate) and poly(ethyl methacrylate) with gas loading. In their work, however, only a limited creep time was chosen. Furthermore, the authors emphasize the effect of so-called retrograde vitrification, whereby a liquid to glass transition takes place with increasing temperature. In summary, a variety of experimental techniques have been developed for investigation of gas loading on thermal, mechanical, and rheological properties of polymers. However, because of the experimental complexity, no routine procedure exists.

In this work, three different methods are applied and compared to determine the glass transition temperature of pristine polystyrene and three related polymers. In addition, a novel construction of a creep test device was tested. The objective of this study is to evaluate the advantages and disadvantages of each technique. In so doing, these three different experimental techniques are compared. The four related different polymers are chosen in order to get insight into the relation between molecular structure and the glass transition temperature.

This work is structured as follows: first, the principles of the three methods for determination of the glass transition temperature T_g are described. Then, experimental data for four different polymers which have a related molecular structure are presented. The results of these different techniques are compared and interpreted considering the specific test parameters and the molecular structure of the homopolymers.

2. Theoretical Foundation of Data Analysis for Determination of T_g

2.1. Differential Scanning Calorimetry. Generally, the specific heat of a polymer is higher above T_g than below T_g. Consequently, a step appears in a differential scanning calorimetry (DSC) curve in the temperature interval around the glass transition and can be straightforward evaluated. However, at elevated atmospheric pressure, the baseline is scattered, and the characteristic step of the glass transition also is visible to a lesser extent. These features restrict DSC measurements by means of conventional DSC apparatus to pressures up to 30 bar. Furthermore, since the actual determination of the glass transition temperature appears in the interval with varying temperature, the exact gas loading can be only approximated. However, an advantage of such measurements is the low amount of necessary material and the generally high accuracy of this technique. In this study, we also present the results of isothermal DSC experiments under gas loading in order to evaluate the saturation time for sorption of carbon dioxide in the polymer.

2.2. Creep Test. In a creep test, the time-dependent deformation (shear or tensile strain) at a constant applied stress is determined. If this test is performed in the elongational mode, the time-dependent tensile creep compliance

$$D(t) = \frac{\varepsilon(t)}{\sigma_{\text{tensile}}} \tag{1}$$

is determined, where t denotes the time, $\varepsilon(t)$ the measured tensile strain, and σ_{tensile} is the applied tensile stress which is constant during the whole creep interval. In this work, this test is performed in the linear range where the measured tensile creep compliance $D(t)$ does not depend on the chosen value of σ_{tensile}.

Because of its viscoelastic nature, the creep compliance increases with time. If initially the polymer sample is in the glassy state, at a certain time interval, a transition from the glassy to the rubbery state takes place. In this interval, the compliance significantly increases and achieves at the end of this time interval the value $D(t_{\text{glass}}) = 1/G_N^o$, where the

plateau modulus is denoted by G_N^o. This equation defines a "time" t_{glass} of glass transition at the chosen measurement temperature. In this work, we focus on the influence of gas loading on the shift of glass transition temperature. If the T_g value at ambient pressure is known, application of the time-temperature superposition principle and the use of an at least phenomenological equation for the temperature-dependence of shift factor at ambient pressure allow one to determine the glass transition temperature at elevated pressure under gas loading. However, in contrast to rheological experiments (which are performed above the glass transition temperature where the Williams-Landel-Ferry (WLF) equation holds for amorphous polymers), this approach also requires creep tests performed below the calorimetric glass transition temperature in order to obtain the functional dependence of the shift factor on temperature below the glass transition temperature.

2.3. Viscosity Measurements. Viscosity measurements allow for the determination of the viscosity reduction caused by the solution of low molecular weight molecules in a polymer sample. In principal, a viscosity reduction corresponds to a shift of glass transition temperature to lower temperatures. The temperature dependence of the viscosity of amorphous polymer melts is generally described by the WLF equation. If the glass transition temperature T_g at ambient pressure is chosen as reference temperature, then the WLF equation for the time-temperature shift factor a_T reads

$$\log(a_T) = -\frac{c_1(T - T_g)}{c_2 + (T - T_g)}, \tag{2}$$

where c_1 and c_2 are material-specific parameters. The zero shear rate viscosity $\eta_0(T)$ at temperature T is given by $\eta_0(T) = a_T\eta_0(T_g)$, where $\eta_0(T_g)$ is the zero shear rate viscosity at the glass transition temperature. Although the time-temperature shift factor $a_T(T_g)$ depends on both the actual temperature T and the glass transition temperature T_g, only the subindex T is generally mentioned. If the glass transition temperature at ambient pressure is known, the use of the WLF equation allows for the determination of T_g at elevated pressures. Using Equation (2), the value of the glass transition temperature $T_{g,p}$ at elevated pressure p can be calculated and is given by

$$T_{g,p} = T - \frac{c_1c_2}{\log(a_T(T_g)a_p) + c_1} + c_2, \tag{3}$$

with the pressure shift factor a_p. Since the WLF parameters at the temperature of glass transition T_g are often not available, the following equation for the reduction ΔT_g of the glass transition temperature caused by pressure and gas loading can be derived from the WLF equation:

$$\Delta T_g = \tilde{c}_2\left[\frac{1}{1 + \tilde{c}_1^{-1}\log(a_T)} - \frac{1}{1 + \tilde{c}_1^{-1}\log(a_Ta_p)}\right], \tag{4}$$

where the WLF parameters $\tilde{c}_1$ and $\tilde{c}_2$ refer to the reference temperature T_{ref}.

3. Experiments and Simulation

3.1. Materials. In this work, four different polymers were used in order to analyze the effect of molecular structure and loading with carbon dioxide (CO_2) on the glass transition temperature T_g. Commercial polymers were chosen for this study. Obviously, the range of available molecular weight averages of commercial products is limited. A polystyrene and three chemically related polymers were selected, namely, poly(2-vinylpyridine), poly(4-vinylpyridine), and poly(α-methyl styrene). The chemical structure of these polymers is depicted in Figure 1, and relevant physical properties are listed in Table 1.

The molecular weight of the polymers was determined by means of gel permeation chromatography (GPC). The samples were dried at 80°C under vacuum before the measurements. The GPC measurements were performed at room temperature in tetrahydrofuran on a Waters instrument (Waters GmbH, Eschborn, Germany), equipped with polystyrene gel columns of pores with size of 10^2, 10^3, 10^4, and 10^5 Å and using a refractive index (RI) detector. Polystyrene of different molecular weights (Polymer Laboratories GmbH, Darmstadt, Germany) was used for calibration.

Thermal gravimetric analysis (TGA) was applied in order to investigate the thermal stability of the materials of this study. The measurements were performed using a TG 209 F1 Libra® (NETZSCH-Gerätebau GmbH, Selb, Germany) in an argon atmosphere.

Before the calorimetric, creep, and rheological experiments, all polymers were dried under vacuum at elevated temperatures for at least 10 hours. The drying temperature and time are listed in Table 2. Whereas polystyrene and poly(α-methyl styrene) were dried below their glass transition temperature, the two hydrophilic polymers (poly(2-vinylpyridine) and poly(4-vinylpyridine)) were dried above their glass transition temperatures in order to reduce residual water.

3.2. Differential Scanning Calorimetry at Ambient and Elevated Pressure. Calorimetric measurements at a constant heating rate were performed in order to measure the glass transition temperature of the homopolymers at ambient and at elevated pressure in a carbon dioxide atmosphere. A DSC apparatus DSC 1 (Mettler-Toledo, Greifensee, Switzerland) for the measurements at ambient pressure and an apparatus HP-DSC 1 (Mettler-Toledo) for the experiments at elevated pressures were used. First, approx. 10 mg of predried powder was filled into a 40 μL aluminum crucible and was sealed with a microperforated lid. The lid was perforated three times with a hole diameter of 50 μm. Afterwards, the crucible with the sample was directly placed into the DSC device, and the measurement was started. Since the system has minor leakages, over long periods of time, the pressure drops permanently during isothermal measurements of about 2 bar/h (maximal allowable pressure drop specified by the supplier 4 bar/h [29]), if there is no constant feed of gas. To perform the experiment under well-defined conditions and to visualize effects

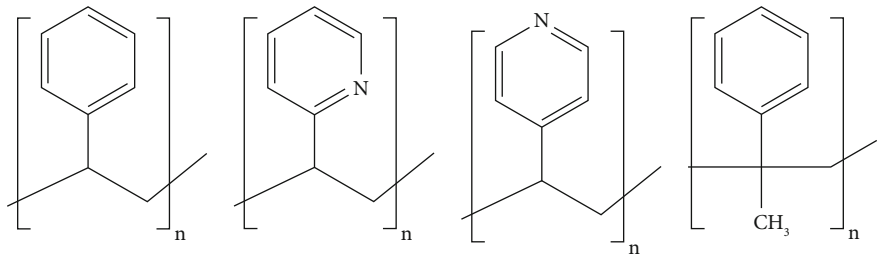

Figure 1: Molecular structure of polystyrene, poly(2-vinylpyridine), poly(4-vinylpyridine), and poly(α-methyl styrene).

Table 1: Number and weight average of the molecular weight (M_n and M_w) and glass transition temperature (T_g) of the polymers of this study.

Polymer	Supplier	M_n (g/mol)	M_w (g/mol)	M_w/M_n	T_g (°C)
Polystyrene PS 158 K (PS)	BASF SE	111 700	253 800	2.27	104
Poly(2-vinylpyridine) (P2VP)	Polymer Source	6 700	18 400	2.76	100
Poly(4-vinylpyridine) (P4VP)	Sigma-Aldrich	45 100	72 800	1.61	150
Poly(α-methyl styrene) (PαMS)	Polymer Source	126 900	128 300	1.01	176

Table 2: Drying temperature T_{dry}, drying time t_{dry}, and temperature of compression moulding T_{press} for the polymers of this study.

Polymer	T_{dry} (°C)	t_{dry} (h)	T_{press} (°C)
Polystyrene PS 158 K	60	>24	180
Poly(2-vinylpyridine)	140	10-48	170
Poly(4-vinylpyridine)	160	10-48	210
Poly(α-methyl styrene)	140	>24	240

during isothermal sorption segments, a very constant pressure level with a deviation of approximately ±0.04 bar during the isothermal segment of about 3 h is required. Therefore, the output pressure of the pressure regulator was set to 2 to 5 bar higher than the test pressure and a minimal flow rate (0.04–0.20 mL/min) was set manually at the inlet to compensate the pressure loss.

In a DSC experiment under elevated pressure, first the polymer sample was heated up to a temperature $T_{max} > T_g$ to eliminate the thermal and mechanical history of the sample. Afterwards, the sample was cooled down to the sorption temperature T_{sorp} which was below the glass transition temperature at ambient pressure. The sorption temperature is listed in Table 3. After achieving the sorption temperature T_{sorp}, the DSC oven was purged with CO_2 for 5 min. Then, the test pressure was applied to the DSC oven and adjusted to the required accuracy. This pressure regulation took approximately 5 min. During this phase, the specimen already absorbs CO_2. Once the pressure was constant, an isothermal sorption segment of 3 h at sorption temperature and test pressure was performed to ensure complete saturation of the polymer. The last interval was a heating cycle from sorption temperature T_{sorp} to temperature T_{max} at a heating rate of 10 K/min to identify the glass transition temperature of the gas-loaded polymer.

Table 3 shows the parameters for the calorimetric measurements of the four homopolymers. Since the signal-noise ratio of the device increases with pressure, only measurements up to a pressure of 30 bar lead to reliable results.

Diffusion and saturation of CO_2 into a polymer is an exothermal, time-dependent process. Consequently, this diffusion process should be visualized during an isothermal sorption interval as a function of heat flow over time. Then, the amount of released heat reduces with time during the sorption period. In order to validate this postulation, different measurements were performed. The first set of experiments investigated the influence of CO_2 on the DSC measurement device itself and time-dependent temperature effects. Therefore, different isothermal measurements were performed. If the postulation is right, from an isothermal sorption measurement for a specific polymer, the time to achieve complete saturation of the polymer can be estimated by the time required to reach a constant heat flow (no heat release or uptake of the specimen). For validation, a specimen was measured with the parameters in Table 3. The isothermal of the second segment was then used for evaluation of the time to complete saturation. Afterwards, the glass transition temperature of the same sample was determined. The length of the sorption intervals was determined on the base of the previously determined time to complete saturation. Two experiments with a shorter sorption time, one experiment with the determined sorption time, and two experiments with a longer sorption time were performed for polystyrene. Between each experiment, a minimum of three hours for desaturation at ambient pressure was assured.

3.3. Rheological Experiments. Rheological experiments were performed using a rotational rheometer (MCR 502, Anton Paar, Graz, Austria). A plate-plate geometry and cylindrical samples were chosen for the investigations. The measurements

were performed above the glass transition temperature of the polymers.

The cylindrical specimens with a diameter of 8 mm and a thickness of 2 mm were compression-moulded under vacuum. For the different materials (pellets and powder, respectively), two different compression-moulding devices were used. For forming the pellets of polystyrene, a pillar press PW 10 H (Paul-Otto Weber GmbH, Remshalden, Germany) was used. The press was preheated to 180°C. Approximately 110 mg of polymer was filled into each of the four cavities of the brass stencil. The stencil was installed in a brass vacuum pan and placed in the press under slight pressure for 150 s. Subsequently, vacuum was applied. After an additional interval of 150 s, the pressing force was increased to 60 kN for another period of 300 s. Afterwards, the specimens were cooled down for at least 30 min holding the pressure and vacuum from the previous step.

The powder of the other three polymers was formed using a vacuum press (MeltPrep GmbH, Graz, Austria). The heating plate was preheated to forming temperature. Approximately 105 mg of polymer was filled into the pressing cylinder and precompacted with the plunger. In the first phase, the vacuum form is closed and placed on the heating plate without applying vacuum. In the second phase, vacuum is applied. Subsequently, the sample is cooled down under vacuum for at least 30 min. The processing temperature for each polymer can be found in Table 2.

Frequency sweeps using poly(α-methyl styrene) and experiments with a constant shear rate for all four polymers were performed at ambient pressure in a nitrogen atmosphere. The time for temperature equilibration was 15 min. In order to determine the linear viscoelastic range of shear oscillations, first an amplitude sweep at an angular frequency of $\omega = 10$ rad/s was carried out. Then, a frequency sweep in the range of angular frequencies ω from 0.01 to 100 rad/s was performed with a shear amplitude γ_0 of 5%. The frequency sweeps started with the highest frequency. By varying the measurement temperature and applying the time-temperature superposition principle, a mastercurve was constructed using the software LSSHIFT in order to determine the WLF parameters [30].

For pressurized rheological measurements, a high-pressure cell (Anton Paar, Graz, Austria) was installed. The pressure cell consists of three major components, i.e., the magnetic cap, the pressure head, and the pressure cup. The pressure cup was installed in the heating system, and the specimen was placed inside. The pressure head contained a pivot-mounted shaft where on the top end a cylindrical magnet and at the lower end the rheological tool were mounted. The upper part was screwed into the lower part of the pressure cell and sealed of the experiment chamber. The magnetic cap was connected to the transducer of the rheometer, connecting the movement of the transducer with the shaft inside the pressure cell. This setup allows to properly seal the experiment chamber even at high pressure.

The principle of the magnetic coupling of the rheological apparatus is presented in Figure 2. Initially, the magnetic coupling is at rest, and all forces are in static equilibrium (Figure 2(a)). For $t > 0$, the macroscopic shear rate (constant angular velocity of the outer magnetic) yields a time-dependent rotation of the inner magnet (Figure 2(b)) until a steady-state situation has been achieved (Figure 2(c)). The magnetic coupling causes a limitation of the accuracy of the time dependence of the viscosity measurements. If the polymer is modelled by a Maxwell element with viscosity η_0 and spring constant G_p, then the magnetic coupling corresponds to an additional Hookean spring in series. This additional spring is associated with elastic constant G_m (see Figure 3). Because of the serial arrangement, the two springs are associated with an effective, single spring constant

$$G_{\text{eff}} = \frac{G_p G_m}{G_p + G_m}, \tag{5}$$

and a relaxation time $\tau_{\text{eff}} = \eta_0(G_p + G_m)/(G_p G_m)$. In a stress-growth experiment, a constant macroscopic shear rate $\dot{\gamma}_0$ is applied which yields for the measured time-dependent viscosity

$$\eta(t) = \eta_0 \left[1 - \exp\left(-\frac{t}{\tau_{\text{eff}}}\right)\right]. \tag{6}$$

The relaxation time of the polymer melt is given by $\tau = \eta_0/G_p$. Consequently, only for $G_m \gg G_p$, the time dependence of the measured torque signal correctly displays the transient response of the polymer melt. On the contrary, the stationary value η_0 is unaffected by the stiffness of the magnetic coupling.

In this work, a plate-plate geometry with a diameter of 20 mm (specimen diameter equal to 8 mm) was used for the experiments in the pressure cell. The time for temperature equilibration was 15 min. Due to the unknown diameter and gap size during the experiment, the shear rate cannot be defined precisely. Furthermore, it is necessary to perform the experiments in the Newtonian regime, where the viscosity is independent on the shear rate, to be able to compare the experiments. On the other hand, the shear rate must be high enough so that the shear stress within the sample can be measured accurately by the transducer. In this work, the experiments were performed with an angular velocity equivalent to a shear rate of $0.01\,\text{s}^{-1}$ for a plate-plate geometry with a diameter of 20 mm and a gap size of 1.0 mm. This setup ensures that the shear rate within the specimen does not exceed the maximum value for the Newtonian regime. After temperature equilibration, a number of tests with constant shear rate were performed. After pressure increase, multiple measurements at a constant shear rate of $0.01\,\text{s}^{-1}$ were performed until the stationary value of the viscosity does not change anymore with time for subsequent individual runs at elevated pressure (see Ref. 22 for details). At this time, the polymer sample is fully saturated with carbon dioxide.

3.4. Creep Experiments under Elevated Pressure. For the high pressure creep test, the standard specimen geometry according to DIN EN ISO 527-2 Type 1BA was chosen [31]. In this work, polystyrene specimens were injection moulded with a Babyplast 6/10P from Christmann Kunststofftechnik GmbH (Kierspe, Germany). The material feed for the machine was

Table 3: Specifications of the HP-DSC experiments.

	PS	P2VP	P4VP	PαMS
T_{sorp} (°C)	50	50	100	140
T_{max} (°C)	200	170	220	240
Test pressure (bar)		10 - 30		
1st segment (air atmosphere)		(i) Heating: 25°C - T_{max} with rate 10 K/min (ii) Cooling: T_{max} to T_{sorp}		
2nd segment (CO_2 atmosphere)		(i) Purging CO_2, 20 mL/min for 5 min (ii) T_{sorp}, test pressure for 3 h (iii) T_{sorp} to T_{max} with rate 10 K/min, test pressure		

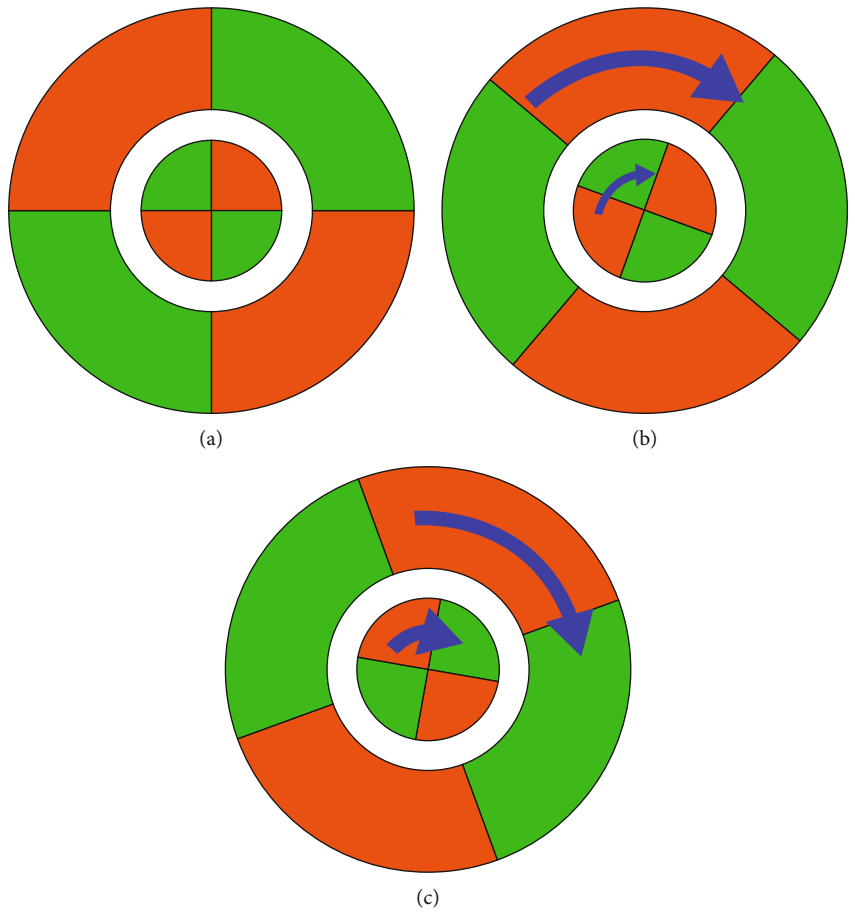

Figure 2: Scheme of the function of the magnetic coupling at deformation with a constant macroscopic shear rate (i.e., a constant angular velocity of the outer magnet). The two colors (orange and green) denote the different poles of the magnet. (a) Magnetic coupling at rest ($t = 0$). (b) Initial phase of shearing with continuously increasing angular velocity of the inner magnet ($t > 0$). (c) Steady-state condition with equal angular velocities of the inner and outer magnet ($t \longrightarrow \infty$).

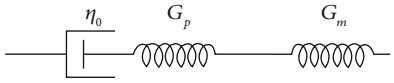

Figure 3: Maxwell model for analysis of the time-dependent response of the magnetic coupling.

dried at 60°C for at least 48 hours. After injection moulding, the specimens were again dried at 60°C for at least 24 hours before they were used for the creep experiments.

A specially designed creep testing device was used for the investigations. The machine is equipped with an autoclave consisting of a fixed pressure flange and a movable pressure dome (see Figures 4(a) and 4(b). These two parts are bolted

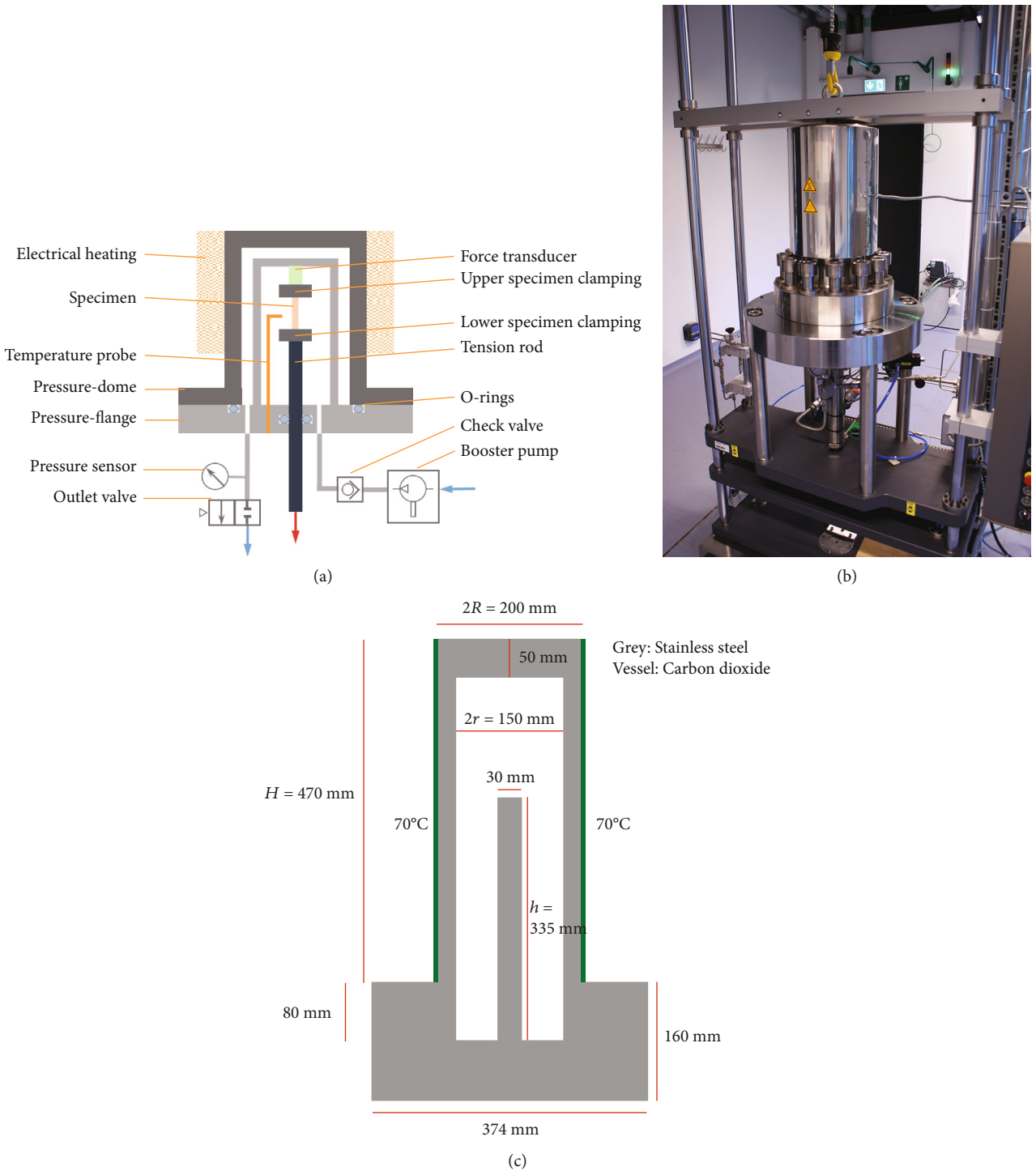

Figure 4: (a) Scheme and (b) photograph of the tensile creep tester. (c) Scheme and dimensions of the vessel of the creep test device with $R = 100$ mm, $H = 470$ mm, $r = 75$ mm, and $h = 335$ mm for the simulations at 70°C.

Table 4: Thermal conductivity λ, density ϱ, and specific heat capacity c_p at constant pressure of carbon dioxide and stainless steel.

Material	λ at 100°C (W/(m K))	ϱ (kg/m^3)	c_p (J/(kg K))	Reference
Carbon dioxide	0.0224	1.98	923	[32]
Stainless steel (grade TP 316/316 L)	15.9	8	500	[33]

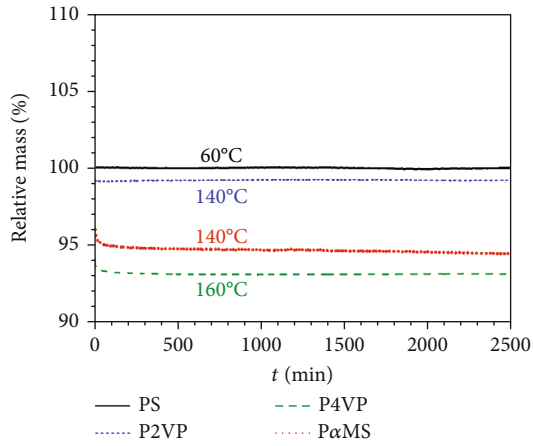

Figure 5: Data of thermal gravimetric analysis at constant temperature in an argon atmosphere. The measurement temperature is indicated.

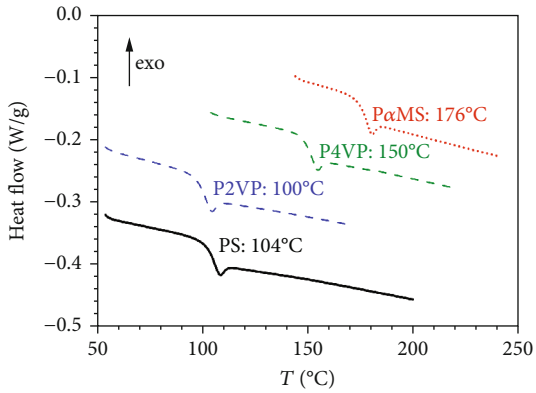

Figure 6: Results of differential scanning calorimetry measurements at ambient pressure. The curves are shifted vertically for clarity.

together. The autoclave can be pressurized with up to 200 bar. To be able to heat the autoclave to maximum 100°C, an electrical one zone heating is installed on the pressure dome. A temperature probe is installed inside the autoclave close to the specimen and is used for the PID controlling of the electrical heating. To be able to fix the specimen, the upper specimen clamping is mounted to an electrical force transducer. The transducer itself is mounted on a rig connected to the pressure flange. The lower specimen clamping is mounted on the tension rod. The tension rod is guided through the pressure flange and can be moved from the outside to apply the load onto the specimen. The movement of the tension rod, and therefore the force applied to the specimen, can be either force or strain controlled. To seal of the autoclave against the pressure, O-rings are installed between the pressure dome and pressure flange as well as between the tension rod and pressure flange. The pressurization is done via a gas bottle connected to a pneumatic piston compressor called booster pump. This allows compressing the gases up to 200 bar and therefore measuring the influence of supercritical CO_2. Right after the booster pump, a check valve is installed to prevent a backflow of the compressed gas out of the autoclave. At the outlet of the autoclave, an electrical pressure sensor is located. The data from this sensor is used for the PID controlling of the booster pump. At the end of the outlet, a pneumatically activated valve is located to be able to depressurize the autoclave.

In this work, experiments with polystyrene specimens were performed, since only polystyrene was available in an amount which is sufficient for injection moulding. First, the specimens were clamped in the device, and the autoclave was closed. Due to the clamping mechanism, the specimen got slightly compressed with a force of approx. 20–40 N. To ensure a defined tensile loading state of the specimen, in the next step, the specimen was preloaded with a tensile load of 2 N. Once the preload is reached, the heating of the autoclave starts automatically. The huge material volume of the autoclave limits the maximum heating rate to 0.5 K/min. Experiments were performed with 30, 50, and 70°C. After reaching the desired temperature and after a saturation time of 72 h for gas loading, the creep load of 50 N was applied automatically, and the measurement was started.

In order to study the spatial homogeneity of the temperature field $T(x, y, z, t)$ in the vessel, finite element simulations were carried out using the software COMSOL Multiphysics® [32]. The geometry of the pressure vessel was slightly simplified. Furthermore, a cylindrical shape of the polymer sample was assumed. The simplified geometry of the device which has been used for the simulations is shown in Figure 4(c). The materials of the colorless and grey domains inside the vessel are carbon dioxide and stainless steel 316 L, respectively. The relevant physical properties of these materials are listed in Table 4.

The wall of the vessel (vertical boundary in green color) is heated at constant temperature. The other outer boundaries are defined by natural convection with air at a temperature of 25°C. This approach requires a convective heat transfer coefficient. A further heat transfer coefficient is used to model the exchange between carbon dioxide and the wall. Because of the rotational symmetry of the vessel, an effective two-dimensional simulation (axisymmetric geometry) is performed with appropriate boundary conditions (vanishing radial gradient) in the center of the vessel.

Because of heating, a laminar flow exists inside the vessel. To model this nonisothermal buoyancy-driven flow, a generalized Navier-Stokes equation that takes into account the variation of density and the energy equation is numerically solved. The buoyancy forces are included by the gravity force.

The fully compressible formulation of the continuity and momentum equations reads

$$\rho\frac{\partial \boldsymbol{v}}{\partial t} + \rho\boldsymbol{v}\bullet\nabla\boldsymbol{v} = -\nabla p + \nabla\bullet\left(\eta\left(\nabla\boldsymbol{v} + (\nabla\boldsymbol{v})^{\mathrm{T}}\right) - \frac{2}{3}\eta(\nabla\bullet\boldsymbol{v})\mathbf{I}\right) + \boldsymbol{F}, \tag{7}$$

where ρ is the density (in kg/m^3), t is the time (in s), $\boldsymbol{v}$ the velocity vector (in m/s), p is the pressure (in Pa), η is the dynamic viscosity (in Pa s), $\mathbf{I}$ is the identity tensor (in Pa),

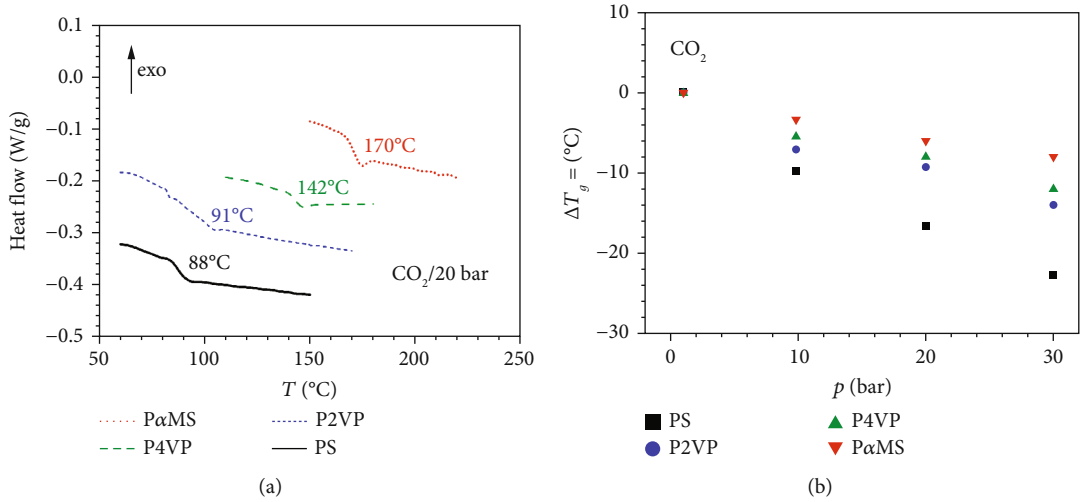

Figure 7: Results of differential scanning calorimetry measurements at elevated pressure. (a) HP-DSC data at a pressure of 20 bar. (b) Reduction ΔT_g of glass transition temperature T_g as a function of pressure p. The curves of heat flow are shifted vertically for clarity.

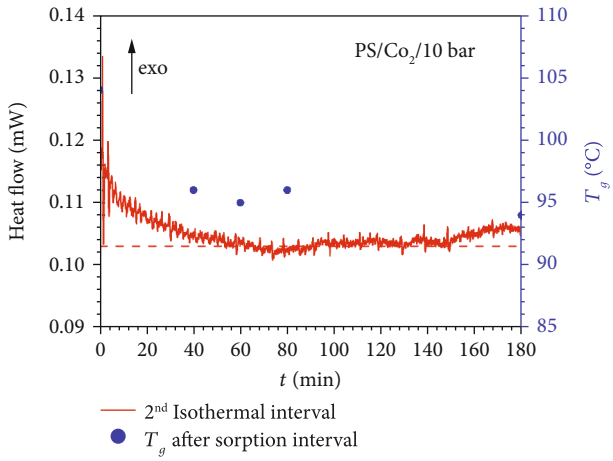

Figure 8: Heat flow and glass transition temperature T_g as a function of sorption time at constant temperature in a HP-DSC device.

and $\boldsymbol{F}$ is the gravity force vector (in N/m^3). Vectors and tensors are written with bold letters.

The velocity field is computed using the laminar flow interface (Navier-Stokes equations). The nonisothermal flow field is calculated by solving the heat and Navier-Stokes equations to determine the velocity and the temperature fields. The heat equation for a fluid is given by

$$\rho c_p \left(\frac{\partial T}{\partial t} + (\boldsymbol{v}\bullet\nabla)T\right) = -(\nabla\bullet\boldsymbol{q}) - \frac{T}{\rho}\frac{\partial \rho}{\partial T}\bigg|_p \left(\frac{\partial p}{\partial t} + (\boldsymbol{v}\bullet\nabla)p\right) + \boldsymbol{Q}, \tag{8}$$

where c_p is the specific heat capacity at constant pressure (in J/(kg K)), T is the absolute temperature (in K), q is the conductive heat flux (in W/m^2), and Q is the heat source (in W/m^3).

This time-dependent equation is solved by use of a heat transfer coefficient h to describe the natural convective cooling on the outer surface of the vessel. This approach is very powerful in many situations, especially if the main interest is not the flow behaviour, but rather its cooling power.

In general, the conductive heat transfer $\dot{Q} = dQ/dt$ is defined by

$$\dot{Q} = \frac{T_1 - T_2}{R}, \tag{9}$$

where $T_1 - T_2$ is the temperature difference and R is the thermal resistance. Taking into account conduction and convection, Equation (9) reads

$$\dot{Q} = \frac{T_3 - T_2}{R_{\text{Conv}}} + \frac{T_1 - T_2}{R_{\text{Cond}}} + \frac{T_{\infty,1} - T_1}{R_{\text{Conv}}}, \tag{10}$$

where $T_3 - T_2$ is the temperature difference because of convection of carbon dioxide, $T_1 - T_2$ is the temperature difference for conduction between the inner and the outer wall of the vessel, and $T_{\infty,1} - T_1$ is the temperature difference because of natural convection of the outer boundary wall and the surrounding air. Furthermore, one has $R_{\text{Conv}} = 1/(hA)$ with the area A and $R_{\text{Cond}} = L/(\lambda A)$ with the thickness L and the thermal conductivity λ.

4. Results and Discussion

4.1. Thermogravimetric Analysis. The results of the thermogravimetric analysis of pristine, undried samples at a constant temperature (i.e., the drying temperature for sample preparation), are presented in Figure 5. The relative mass only slightly decreases in the beginning of the experiments and then stays constant in the chosen time interval. These data show that the chosen drying temperatures do not lead to a significant decrease of relative mass, and consequently, no significant degree of degradation takes place.

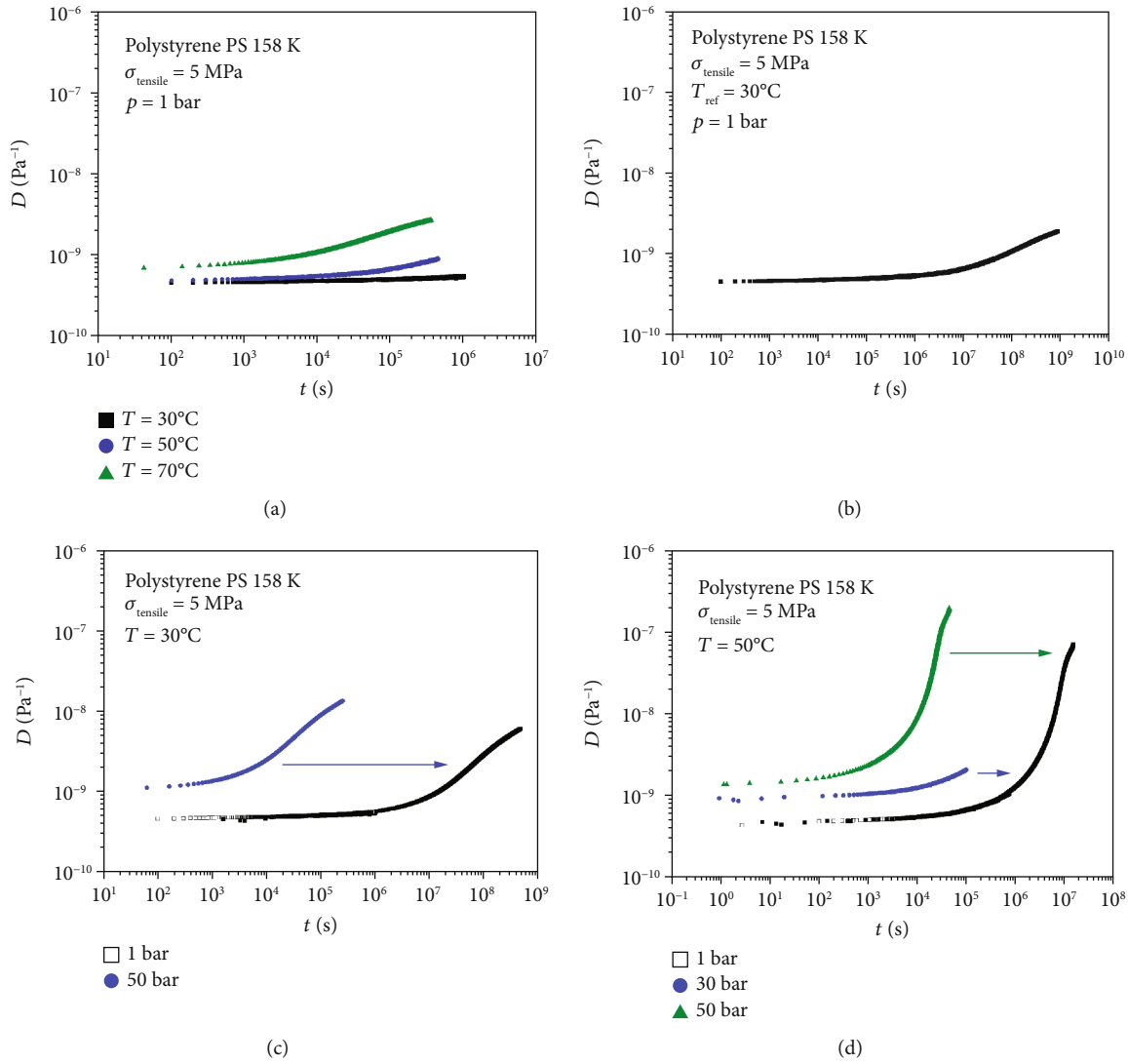

Figure 9: Time-dependent tensile creep compliance $D(t)$ of polystyrene PS 158 K at various temperatures and pressures. (a) Tensile creep compliance at a pressure of 1 bar and temperatures of 30, 50, and 70°C. (b) Mastercurve of the data in (a). (c) Creep compliance at a temperature of 30°C and pressures of 1 and 50 bar as well as the mastercurve for a pressure of 1 bar. (d) Creep compliance at a temperature of 50°C and pressures of 1, 30, and 50 bar as well as the mastercurve for a pressure of 1 bar. In (c) and (d), the data of the mastercurves appear in black color.

4.2. Calorimetric Experiments. Figure 6 shows the measured heat flow for the four different polymers of this study at ambient pressure. Polystyrene (T_g = 104°C) and poly(2-vinylpyridine) (T_g = 100°C) are associated with similar glass transition temperatures which indicates that the nitrogen atom in poly(2-vinylpyridine) does not influence the free volume very much. On the contrary, the glass transition temperatures of poly(4-vinylpyridine) and poly(α-methyl styrene) are significantly higher because of the more pronounced influence of the electrophilic nitrogen atom in poly(4-vinylpyridine) and the bulky methyl group in poly(α-methyl styrene), respectively. Figure 7(a) reveals that the glass transition temperature under an elevated CO_2 pressure (here as an example of 20 bar) is reduced for all four homopolymers. The maximum test pressure in our DSC experiments was limited to 30 bar. Interestingly, polystyrene is associated with the largest reduction of glass transition temperature of the four homopolymers of this study (Figure 7(b)). Poly(α-methyl styrene) reveals the lowest reduction of glass transition temperature at elevated CO_2 pressure, possibly because of the presence of the methyl group. Multiple measurements reveal a good reproducibility.

The result of an isothermal sorption experiment was exemplified for a CO_2 pressure of 10 bar and is presented in Figure 8. In the beginning at time zero, the heat flow attains its maximum and then decays to zero. It has been experimentally verified that this small heat flow is not an experimental artefact by performing tests with no or an empty crucible and by adding an additional time interval (see the second isothermal interval in Figure S1 of the Supplementary Materials).

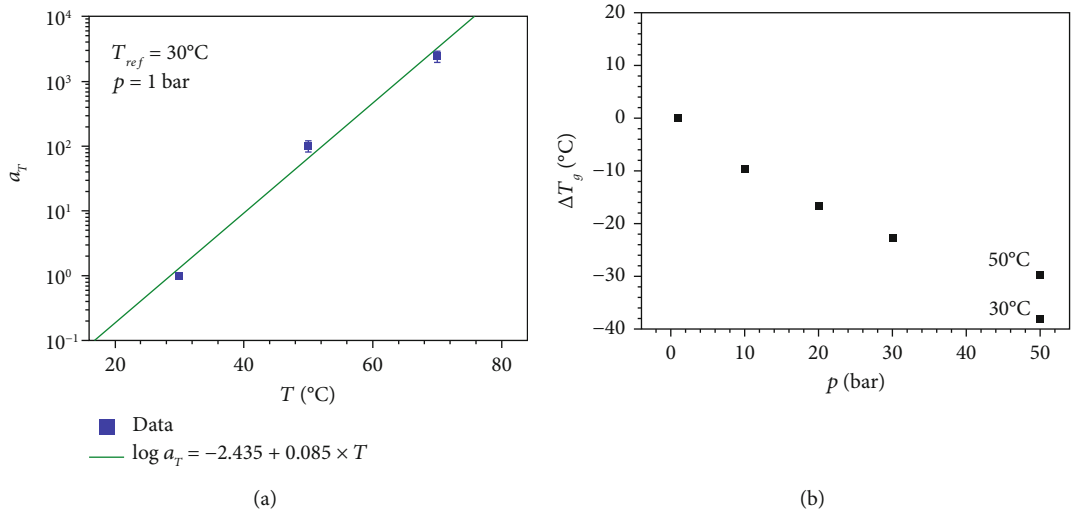

(a) (b)

Figure 10: (a) Calculated shift factor a_T as obtained by tensile creep experiments at 30°C and ambient pressure. The result of a linear fit to the data is also plotted. (b) Glass transition temperature as a function of applied pressure as determined by analysis of the tensile creep compliance and of DSC experiments.

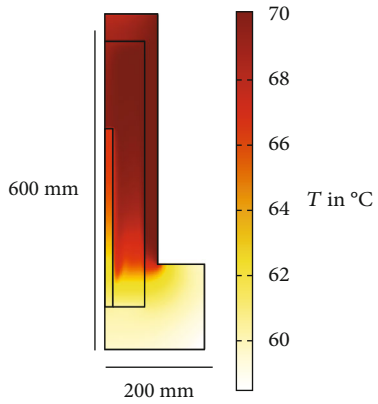

Figure 11: Stationary temperature field as obtained by numerical simulations of the heat equation at a heating temperature of 70°C.

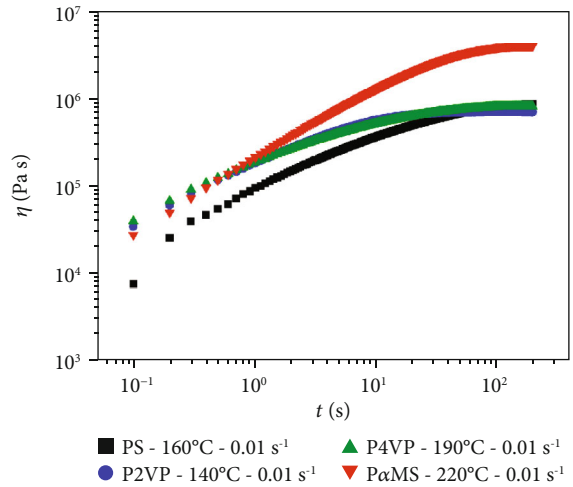

Figure 12: Results of stress-growth experiments at a shear rate of 0.01 s^{-1} and ambient pressure (1 bar). The measurement temperature is indicated. The polymers are polystyrene, poly(2-vinylpyridine), poly(4-vinylpyridine), and poly(α-methyl styrene).

The heat flow in these isothermal sorption experiments is caused by the continuous solution of CO_2 molecules in the polymer phase. Figure S2 of the Supplementary Materials reveals the decay of heat flow at a pressure of 10 bar until complete sorption of CO_2. This process is an exothermal process. The length of the isothermal interval was varied for polystyrene. After the sorption experiment, the glass transition temperature was determined in a heating cycle with a heating rate of 10 K/min and is also shown in Figure 8 for different lengths of the isothermal sorption interval. The visual end of a significant heat flow corresponds to the measured, lowest value of T_g. This result confirms our argumentation that the measured heat flow is caused by the gas sorption process.

4.3. Creep Experiments. In the creep tests, the applied tensile stress σ_{tensile} was set to 5 MPa. Figure 9 presents the time-dependent creep compliance $D(t)$ in the elongational mode for different temperature and pressure values. The chosen time interval of our creep measurements corresponds to the glassy regime and the onset of the transition region. Figure 9(a) presents the creep compliance at different temperatures and ambient pressure. The creep compliance increases with time and also with temperature. The data for 70°C at ambient pressure are in good agreement with the measurements of Schwarzl and Zahradnik [34]. By applying the time-temperature superposition principle and the software LSSHIFT [29], a mastercurve for the time-dependent creep compliance $D(t)$ can be constructed (see Figure 9(b)). Figure 9(c) presents the creep compliance at 30°C and ambient pressure and a pressure of 50 bar, respectively. A higher pressure implies a higher gas loading. A higher temperature and a higher gas loading caused by the

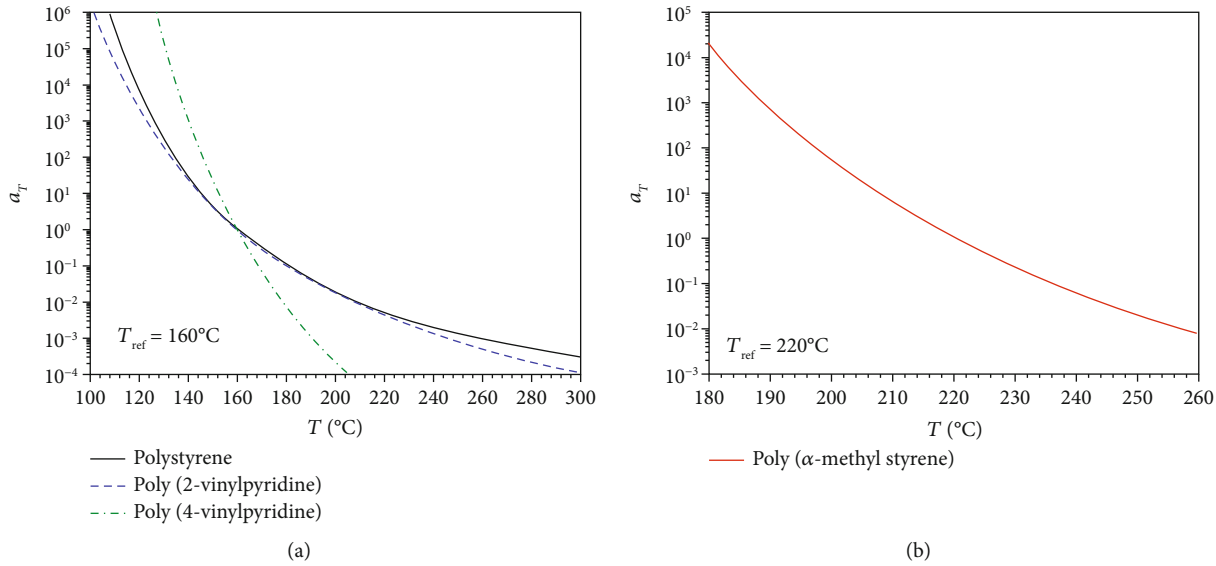

Figure 13: Shift factor calculated using the WLF equation for the four polymers of this study. The reference temperature T_{ref} is (a) 160°C and (b) 220°C.

Table 5: Parameters of the WLF equation at the reference temperature T_{ref} (cf. remark below Equation (4)).

Polymer	$\tilde{c}_1$	$\tilde{c}_2$ (°C)	T_{ref} (°C)	Reference (WLF parameters)
Polystyrene	6.2	105.2	160	[35]
Poly(2-vinylpyridine)	7.63	131.9	160	[36]
Poly(4-vinylpyridine)	13.4	106.2	160	[35]
Poly(α-methyl styrene)	8.4	117.4	220	This work

higher pressure have similar effects: they both lead to an increase of the creep compliance in such a way that it corresponds to a shift of the creep curves towards smaller times. Therefore, a mastercurve can be constructed which is also shown in Figure 9(c). A similar procedure for measurements at a temperature of 50°C with pressure values of 1 bar, 30 bar, and 50 bar is shown in Figure 9(d).

For analysis of the glass transition temperature, the shift factor a_T determined by creep tests at ambient pressure was used (Figure 10(a)). Since the measurement temperature was far below the glass transition temperature of polystyrene at ambient pressure, an empirical fit to the experimental data was applied. The shift factors measured at different temperatures and pressures were recalculated to the reference parameters (30°C and 1 bar) by multiplying the shift factor with respect to pressure at the measurement temperature and the shift factor with respect to the reference temperature of 30°C. Then, the data in Figure 10(a) are used for determination of the effective temperature T_{eff} based on the calculated shift factor which is the product of pressure and temperature (with respect to the reference temperature of 30°C) shift factors. The difference of 30°C and the effective temperature T_{eff} yield the reduction of glass transition temperature $\Delta T_g = 30°C - T_{eff}$. The results are presented in Figure 10(b) together with the DSC data for polystyrene. The data reveal that the glass transition temperature decreases with increasing pressure at the chosen temperature and pressure values. An approximately linear trend holds in the presented pressure range.

The results of the simulations of the temperature field in the vessel for a set temperature of 70°C are displayed in Figure 11. The simulations show that an almost uniform temperature distribution is achieved by the chosen construction. In the experiment, an isolating cover has been additionally used in order to improve temperature homogeneity.

4.4. Rheology. Generally, two effects lead to a change of the glass transition temperature T_g in CO_2-loaded polymers, namely, the effect of pressure (which tends to increase the value of T_g) and the CO_2 concentration (which tends to reduce the T_g value). The presence of a hydrostatic pressure solely yields to an increase of zero shear rate viscosity η_0 which is quantified by the pressure coefficient β

$$\beta = \frac{1}{\eta_0}\left(\frac{d\eta_0}{dp}\right)_T. \quad (11)$$

After an increase of pressure p, the value of the stationary viscosity increases which is described by the pressure coefficient β. A literature value for a linear polystyrene is given by 51.6 GPa^{-1} [15]. Taking a value of $\beta = 50\ GPa^{-1}$, a

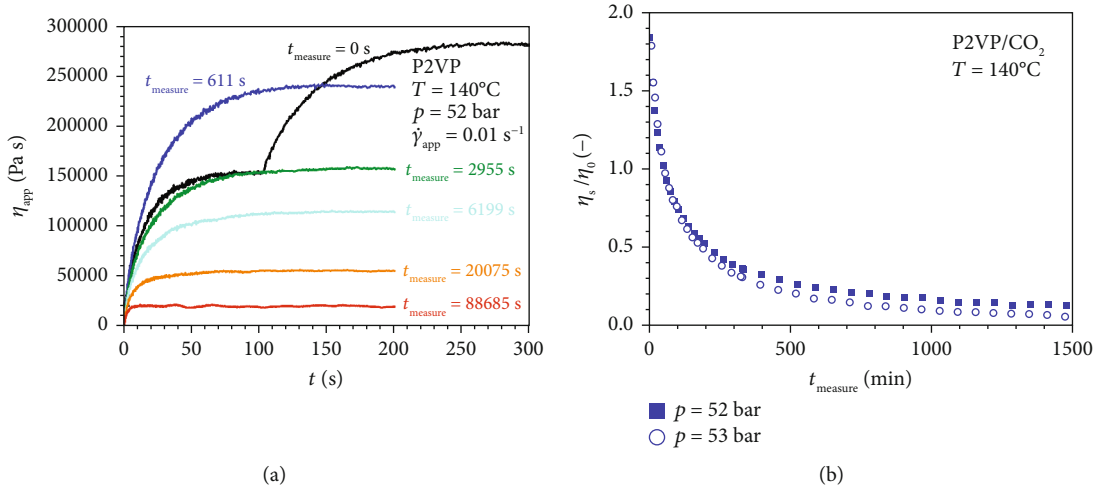

FIGURE 14: Example of a typical rheological experiment at high pressure in a CO_2 atmosphere (P2VP, 140°C, 52 bar CO_2). (a) Apparent time-dependent shear viscosity $\eta_{app}(t)$ at different times after pressure increase. (b) Variation of steady-state viscosity η_s (relative value with respect to zero shear rate viscosity η_0 at ambient pressure) with measurement time $t_{measure}$.

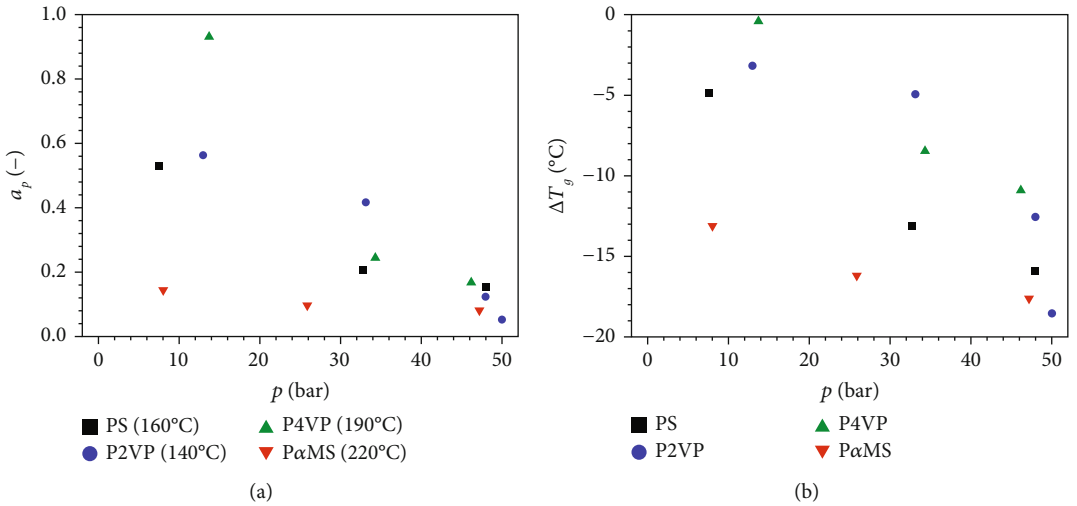

FIGURE 15: Influence of carbon dioxide loading on (a) relative reduction $\eta_s(p)/\eta_s(1\,\text{bar})$ of the steady-state viscosity η_s and (b) reduction of the glass transition temperature T_g of the four polymers of this study as determined by rheological experiments.

pressure increase of 19 bar (i.e., from ambient pressure to 20 bar) yields a viscosity increase of 10%.

Figure 12 presents the results of stress-growth experiments at ambient pressure using the rheometer in the conventional setup (no pressure cell). The chosen low shear rate of 0.01 s^{-1} corresponds to the linear regime. The steady-state viscosity is in a similar range for all four homopolymers at the chosen test parameters. The two homopolymers poly(2-vinylpyrindine) and poly(4-vinylpyrindine) have a lower molecular weight than the other two polymers and thus are associated with a smaller average relaxation time. This is evident from Figure 12, since poly(2-vinylpyrindine) and poly(4-vinylpyrindine) attain a stationary state at shorter times.

The temperature dependence of the shift factor a_T (WLF equation) is shown in Figure 13. The used WLF parameters are listed in Table 5. Polystyrene and poly(2-vinylpyrindine) are associated with a similar shift behaviour in contrast to poly(4-vinylpyridine) and poly(α-methyl styrene). The data reveal that a shift of a_T by a factor of ten corresponds to a temperature change in the order of 20°C. This implies that the statistical scattering of rheological experiments is associated with an error in the order of a few degrees Celsius.

The results of the subsequent stress-growth tests for poly(2-vinylpyridine) at high pressure is depicted in Figure 14. The increase of pressure from ambient pressure to the set high pressure at measurement time $t_{measure} = 0$ and $t = 100$ s can be clearly seen by the increase of viscosity in the stress-growth curve (Figure 14(a)). The multiple runs with constant shear rate are subsequently performed. Because of continuous diffusion of carbon dioxide into the polymer, the stationary value of viscosity decreases with increasing measurement time (Figure 14(b)).

The influence of pressure on viscosity reduction and shift of glass transition temperature is depicted in Figure 15. The solution of carbon dioxide in the polymer melt yields a significant reduction of viscosity (Figure 15(a)). Since the solubility of carbon dioxide in polymers is lower above their glass transition temperature than below T_g, the reduction of glass transition temperature as determined by the rheological experiments is smaller than the values determined by HP-DSC and the creep experiments (Figures 5(b) and 8(b)). In addition, in our experiments, a different behaviour for poly(α-methyl styrene) in HP-DSC and rheological experiments is observed. A possible reason for this experimental phenomenon may be that temperature and gas loading have a different impact on plastification of the polymer. Consequently, poly(α-methyl styrene) does not seem to be behave baro-thermorheological simple.

5. Conclusion

Three different experimental methods were compared to investigate the properties of polystyrene and three related polymers under carbon dioxide loading and at elevated pressure. Differential scanning calorimetry measurements are often limited to a pressure of 30 bar for polymers. In contrast to the mechanical and rheological methods of this study, DSC measurements are performed under nonisothermal conditions which implies a nonconstant gas concentration. Mechanical and rheological test devices at high gas pressure are run at isothermal conditions. Rheological tests using a rotational rheometer are associated with the drastic change of measured torque because of gas loading. In this work, a novel commercial creep testing device has been tested. Simulations reveal an almost uniform temperature field in the vessel of the creep testing device up to 70°C. The overall performance of the device allows the reliable acquisition of the time-dependent creep compliance. In particular, the device can work far below the glass transition temperature of the polymer at ambient pressure. In our experiments, the measured reduction of glass transition temperature of polystyrene in DSC and creep experiments was larger than for poly(2-vinylpyridine) and poly(4-vinylpyridine). The creep experiments of this study extend the pressure range of DSC measurements. The measured data for polystyrene of DSC and creep experiments complement each other very well. Poly(α-methyl styrene) was associated with a different behaviour in calorimetric and rheological experiments under gas loading and therefore shows a more complex behaviour.

Data Availability

The data that support the findings of this study are available from the corresponding author upon reasonable request.

Disclosure

Felix Harden present address is Technische Hochschule Lübeck, Department of Mechanical Engineering and Business Administration, Mönkhofer Weg 239, 23562 Lübeck, Germany. Mahboubeh Kargar present address is SUZLON Energy Ltd., Department for Innovation and Strategic Research, Hamburg, Germany. Ulrich A. Handge present address is TU Dortmund University, Faculty of Mechanical Engineering, Chair of Plastics Technology, Leonhard-Euler-Strasse 5, 44227 Dortmund, Germany.

Conflicts of Interest

The authors declare that they have no conflicts of interest.

Authors' Contributions

Felix Harden was responsible for the experiments, analysis, and writing of the manuscript. Mahboubeh Kargar was responsible for the simulations, analysis, and writing of the manuscript. Ulrich A. Handge was responsible for the experiments, analysis, writing of the manuscript, and conceptualisation.

Acknowledgments

The discussions with Prof. Dr. Volker Abetz and Dr. Thomas Leitgeb-Simandl are gratefully acknowledged. The authors thank Mrs. Maren Brinkmann, Mr. Kristian Buhr, Dr. Jelena Lillepärg, Mr. Silvio Neumann, Mrs. Melanie Reyes, and Mrs. Ivonne Ternes for the experimental support.

Supplementary Materials

Data are provided to show that the measured decay of heat flow during the isothermal sorption interval is not an experimental artefact. *(Supplementary Materials)*

References

[1] R. P. White and J. E. G. Lipson, "Polymer free volume and its connection to the glass transition," *Macromolecules*, vol. 49, no. 11, pp. 3987–4007, 2016.

[2] J. S. Chiou, J. W. Barlow, and D. R. Paul, "Plasticization of glassy polymers by CO_2," *Journal of Applied Polymer Science*, vol. 30, no. 6, pp. 2633–2642, 1985.

[3] Y. Mi and S. Zheng, "A new study of glass transition of polymers by high pressure DSC," *Polymer*, vol. 39, no. 16, pp. 3709–3712, 1998.

[4] D. Raps, T. Köppl, A. R. de Anda, and V. Altstädt, "Rheological and crystallisation behaviour of high melt strength polypropylene under gas-loading," *Polymer*, vol. 55, no. 6, pp. 1537–1545, 2014.

[5] D. Raps, T. Köppl, L. Heymann, and V. Altstädt, "Rheological behaviour of a high-melt-strength polypropylene at elevated pressure and gas loading for foaming purposes," *Rheologica Acta*, vol. 56, no. 2, pp. 95–111, 2017.

[6] M. Wessling, S. Schoeman, T. van der Boomgaard, and C. A. Smolders, "Plasticization of gas separation membranes," *Gas Separation and Purification*, vol. 5, no. 4, pp. 222–228, 1991.

[7] M. Kargar and U. A. Handge, "Numerical simulations of gas sorption experiments in polymers: influence of aspect ratio and pressure increase rate on the determination of diffusion coefficient," *Macromolecular Theory and Simulations*, vol. 30, no. 5, p. 2100016, 2021.

[8] I. C. Sanchez and P. A. Rodgers, "Solubility of gases in polymers," *Pure and Applied Chemistry*, vol. 62, no. 11, pp. 2107–2114, 1990.

[9] K. F. Webb and A. S. Teja, "Solubility and diffusion of carbon dioxide in polymers," *Fluid Phase Equilibria*, vol. 158-160, pp. 1029–1034, 1999.

[10] P. Kundra, S. R. Upreti, A. Lohi, and J. Wu, "Experimental determination of composition-dependent diffusivity of carbon dioxide in polypropylene," *Journal of Chemical and Engineering Data*, vol. 56, no. 1, pp. 21–26, 2011.

[11] Y. Sato, T. Takikawa, S. Takishima, and H. Masuoka, "Solubilities and diffusion coefficients of carbon dioxide in poly(vinyl acetate) and polystyrene," *Journal of Supercritical Fluids*, vol. 19, no. 2, pp. 187–198, 2001.

[12] J. Wilmers and S. Bargmann, "Simulation of non-classical diffusion in polymers," *Heat and Mass Transfer*, vol. 50, no. 11, pp. 1543–1552, 2014.

[13] L. Kulisiewicz and A. Delgado, "High-pressure rheological measurement methods: a review," *Applied Rheology*, vol. 20, no. 1, pp. 13011–13018, 2010.

[14] P. D. Driscoll and D. C. Bogue, "Pressure effects in polymer melt rheology," *Journal of Applied Polymer Science*, vol. 39, no. 8, pp. 1755–1768, 1990.

[15] H. E. Park, J. Dealy, and H. Münstedt, "Influence of long-chain branching on time-pressure and time-temperature shift factors for polystyrene and polyethylene," *Rheologica Acta*, vol. 46, no. 1, pp. 153–159, 2006.

[16] H. E. Park, S. T. Lim, H. M. Laun, and J. M. Dealy, "Measurement of pressure coefficient of melt viscosity: drag flow versus capillary flow," *Rheologica Acta*, vol. 47, no. 9, pp. 1023–1038, 2008.

[17] N. M. Rudolph, A. C. Agudelo, J. C. Granada, H. E. Park, and T. A. Osswald, "WLF model for the pressure dependence of zero shear viscosity of polycarbonate," *Rheologica Acta*, vol. 55, no. 8, pp. 673–681, 2016.

[18] C. Reynolds, R. Thompson, and T. McLeish, "Pressure and shear rate dependence of the viscosity and stress relaxation of polymer melts," *Journal of Rheology*, vol. 62, no. 2, pp. 631–642, 2018.

[19] H. Münstedt, "Influence of hydrostatic pressure on rheological properties of polymer melts - a review," *Journal of Rheology*, vol. 64, no. 3, pp. 751–774, 2020.

[20] J. R. Royer, Y. J. Gay, J. M. Desimone, and S. A. Khan, "High-pressure rheology of polystyrene melts plasticized with CO_2: experimental measurement and predictive scaling relationships," *Journal of Polymer Science B: Polymer Physics*, vol. 38, no. 23, pp. 3168–3180, 2000.

[21] M. J. Wingert, S. Shukla, K. W. Koelling, D. L. Tomasko, and L. J. Lee, "Shear viscosity of CO_2-plasticized polystyrene under high static pressures," *Industrial and Enginering Chemical Research*, vol. 48, no. 11, pp. 5460–5471, 2009.

[22] U. A. Handge and V. Altstädt, "Viscoelastic properties of solutions of polystyrene melts and carbon dioxide: analysis of a transient shear rheology approach," *Journal of Rheology*, vol. 56, no. 4, pp. 743–766, 2012.

[23] J. Wang, D. F. James, and C. B. Park, "Planar extensional flow resistance of a foaming plastic," *Journal of Rheology*, vol. 54, no. 1, pp. 95–116, 2010.

[24] S. A. E. Boyer and J.-P. E. Grolier, "Modification of the glass transitions of polymers by high-pressure gas solubility," *Pure and Applied Chemistry*, vol. 77, no. 3, pp. 593–603, 2005.

[25] E. Huang, X. Liao, C. Zhao, C. B. Park, Q. Yang, and G. Li, "Effect of unexpected CO_2's phase transition on the high-pressure differential scanning calorimetry performance of various polymers," *ACS Sustainable Chemistry and Engineering*, vol. 4, no. 3, pp. 1810–1818, 2016.

[26] C. Tsioptsias and C. Panayiotou, "Simultaneous determination of sorption, heat of sorption, diffusion coefficient and glass transition depression in polymer-CO_2 systems," *Thermochimica Acta*, vol. 521, no. 1-2, pp. 98–106, 2011.

[27] W.-C. V. Wang, E. J. Kramer, and W. H. Sachse, "Effects of high-pressure CO_2 on the glass transition temperature and mechanical properties of polystyrene," *Journal of Polymer Science: Polymer Physics Edition*, vol. 20, no. 8, pp. 1371–1384, 1982.

[28] P. D. Condo and K. P. Johnston, "In situ measurement of the glass transition temperature of polymers with compressed fluid diluents," *Journal of Polymer Science B: Polymer Physics*, vol. 32, no. 3, pp. 523–533, 1994.

[29] Mettler-Toledo, *TA Logbook Module HP DSC 1*, A. G. Mettler-Toledo, Ed., Mettler-Toledo AG, Greifensee (Switzerland), 2010.

[30] J. Honerkamp and J. Weese, "A note on estimating master-curves," *Rheologica Acta*, vol. 32, no. 1, pp. 57–64, 1993.

[31] *International Organization for Standardization (ISO) DIN EN ISO 527 - Plastics: Determination of tensile properties*, International Organization for Standardization (ISO), Central Secretariat, Geneva, Switzerland, 2019.

[32] "COMSOL Multiphysics® GmbHGöttingen, Germany.

[33] P. G. Klemens, G. Neuer, B. Sundqvist, C. Uher, and G. K. White, "Thermal conductivity of pure metals and alloys," in *Landolt-Börnstein: Numerical Data and Functional Relationships in Science and Technology Volume 15c*, O. Madelung and G. K. White, Eds., Springer, Berlin, 1991.

[34] F. R. Schwarzl and F. Zahradnik, "The time temperature position of the glass-rubber transition of amorphous polymers and the free volume," *Rheologica Acta*, vol. 19, no. 2, pp. 137–152, 1980.

[35] M. Schulze, U. A. Handge, and V. Abetz, "Preparation and characterisation of open-celled foams using polystyrene-*b*-poly(4-vinylpyridine) and poly(4-methyl styrene)-*b*-poly(4-vinylpyridine) diblock copolymers," *Polymer*, vol. 108, pp. 400–412, 2017.

[36] Y. Takahashi, N. Ochiai, Y. Matsushita, and I. Noda, "Viscoelastic properties of poly(2-vinylpyridine) in bulk and solution," *Polymer Journal*, vol. 28, no. 12, pp. 1065–1070, 1996.